

A Novel Synthesis Method of a Sparse Rectangular Planar Receiving Array for Microwave Power Transmission

Jianxiong Li^{1, 2, *} and Shuo Liu^{1, 2}

Abstract—A novel synthesis method of a sparse rectangular planar receiving array (SRPRA) to maximize the power transmission efficiency (*PTE*) for microwave power transmission (MPT) is proposed in this paper. The array element positions of the SRPRA are symmetrically distributed among different quadrants such that the array elements at symmetrical positions receive the same power, and the SRPRA adopts a sparse layout. This reduces the number of array elements and simplifies the complexity of the feeding network. An improved adaptive chaotic particle swarm optimization (IACPSO) algorithm is proposed for the optimization synthesis problem of the SRPRA. Through the optimization of the proposed IACPSO algorithm, the optimal element layout of the SRPRA can be obtained efficiently to get the maximum *PTE*. In addition, we conduct a series of simulation experiments to verify the advantages of the proposed SRPRA model and the effectiveness of the IACPSO algorithm. Firstly, we analyze the effects of different parameters on the synthesis results of the SRPRA. Secondly, comparing the results with those of the sparse random circular aperture array (SRCAA), it is demonstrated that the SRPRA synthesized with the IACPSO algorithm can obtain higher *PTE* with fewer elements and has a relatively simple feeding network. Finally, compared with the standard particle swarm optimization (PSO) algorithm, the proposed IACPSO algorithm can effectively and stably obtain the synthesis results of the SRPRA under different parameters. Therefore, the SRPRA is suitable for creating an efficient MPT system.

1. INTRODUCTION

Microwave power transmission (MPT) is a long-distance energy transmission technology that transmits energy in the form of electromagnetic waves from the transmitting end to the receiving end without using wires, cables, and other physical carriers [1–3]. This energy transmission mode gets rid of the constraints of the traditional energy transmission mode that is vulnerable to terrain and other environmental factors, so it is also more widely used. In addition to being used in the High-Altitude Air (HAA) ship and Space Solar Power Satellite (SSPS) programs, it can also be used for microwave-driven wearable devices, implantable medical devices, electric vehicles, and wireless transmission in remote mountainous areas [4–7].

The MPT system consists of three main components: microwave power generator, microwave transmitting antenna, microwave receiving and rectifying antenna [8]. The efficiency of the system depends on the product of microwave conversion efficiency in the transmitting antenna subsystem, energy transmission efficiency in the free transmission space, and microwave rectification efficiency in the receiving antenna subsystem [9, 10]. The main research of this paper is the layout of the array element positions in the receiving antenna subsystem. The power transmission efficiency (*PTE*) is an important performance index to measure the antenna receiving efficiency [11], which is defined as the

Received 17 April 2023, Accepted 14 June 2023, Scheduled 26 June 2023

* Corresponding author: Jianxiong Li (lijianxiong@tiangong.edu.cn).

¹ School of Electronics and Information Engineering, Tiangong University, Tianjin, China. ² Tianjin Key Laboratory of Optoelectronic Detection Technology and Systems, Tianjin, China.

ratio of the power received by the receiving array to the power transmitted by the transmitting array [12]. Currently, many studies have focused on the aperture illumination distribution of the transmitting and receiving antennas [13–15]. However, there are few studies on the use of receiving antenna array elements to calculate the received power. Therefore, based on the study on the location layout of the receiving array elements, we propose a sparse rectangular planar receiving array (SRPRA) model in this paper. To accurately calculate the received power, the model uses the method that is derived based on the superposition of the electric fields radiated from individual transmitter (Tx) elements and captured by each receiver (Rx) element [16].

In [17], a sparse random circular aperture array (SRCAA) is proposed, in which elements satisfying the minimum array element spacing are randomly distributed under a circular aperture, and then the positions of the array elements are optimized by the standard particle swarm optimization (SPSO) algorithm to improve the *PTE*. Due to the random distribution of each array element in the SRCAA, the received power of the array element is different. Therefore, the array needs to be equipped with amplifiers and phase shifters for each array element, which increases the complexity of the feeding network in the receiving array [18, 19]. To simplify the array feeding network and reduce the system cost, the SRPRA is proposed in this paper, whose array elements are sparse and symmetrically distributed in each quadrant, so that the received power of the array elements at symmetric positions is the same. As a result, the number of array elements is reduced, while the complexity of the feeding circuit is also reduced. In addition, to optimize the layout of the SRPRA, an improved adaptive chaotic particle swarm optimization (IACPSO) algorithm is proposed in this paper [20–24]. To address the shortcoming that the SPSO algorithm may be trapped in a local optimal solution, we propose a new strategy of adaptive inertia weights and learning factors to improve the global traversal and global search. Then, based on the proposed IACPSO algorithm, we conduct a large number of simulation experiments to verify the advantages of the SRPRA model. Compared with the SRCAA, the SRPRA optimized by the IACPSO algorithm can obtain higher *PTE* with fewer array elements for the same aperture size, so that the feeding network is relatively simple, which can reduce the system cost. In summary, this verifies the validity of the model and synthesis method proposed in this study.

2. MATHEMATICAL DERIVATION OF THE MAXIMUM *PTE* OF THE SRPRA

The system model of the MPT is shown in Fig. 1. It is divided into a Tx array located in the XOY plane and an Rx array located in the $X'O'Y'$ plane. Here, it is assumed that there is no obstacle between the Tx array and Rx array. The numbers of array elements in Tx and Rx are Nt and Nr , respectively. The coordinate of the m -th Tx element is $(x_{t,m}, y_{t,m}, z_{t,m})$, and $z_{t,m} = 0$. The aperture size of the receiving array is $L_x \times L_y$, and the minimum array element spacing is defined as d_{\min} . The coordinate position of the n -th Rx element can be set as $(x_{r,n}, y_{r,n}, z_{r,n})$, $z_{r,n} = L$, and L is the distance between the Tx array and Rx array.

According to [16], the received power (P_{r_n}) of the n -th Rx element can be expressed as

$$P_{r_n} = \left(\frac{\lambda}{4\pi} \right)^2 \left| \sum_{m=1}^{Nt} \sqrt{P_{t_m} G_{t_m}(\theta_{n,m}, \phi_{n,m}) G_{r_n}(\theta_{n,m}, -\phi_{n,m})} \frac{e^{-j(kR_{n,m} - \beta_m)}}{R_{n,m}} \right|^2 \quad (1)$$

where λ represents the wavelength in free space, k the wave-number, P_{t_m} the excitation power of the m -th Tx element, $G_{t_m}(\theta_{n,m}, \phi_{n,m})$ the realized gain of the co-polarization of the m -th Tx element in the direction of the n -th Rx element, $G_{r_n}(\theta_{n,m}, -\phi_{n,m})$ the realized gain of the co-polarization of the n -th Rx element in the direction of the m -th Tx element, β_m the excited phase of the m -th Tx element, and $R_{n,m}$ the relative distance between the n -th Rx element and the m -th Tx element, which is written as

$$R_{n,m} = \sqrt{(x_{r,n} - x_{t,m})^2 + (y_{r,n} - y_{t,m})^2 + (z_{r,n} - z_{t,m})^2} = \sqrt{(x_{r,n} - x_{t,m})^2 + (y_{r,n} - y_{t,m})^2 + L^2} \quad (2)$$

Assuming that this principle applies equally to all Nr elements in the Rx array, the received individual power is synthesized without loss. Then the total received power (P_R) can be expressed as

$$P_R = \sum_{n=1}^{Nr} P_{r_n} = \left(\frac{\lambda}{4\pi} \right)^2 \sum_{n=1}^{Nr} \left| \sum_{m=1}^{Nt} \sqrt{P_{t_m} G_{t_m}(\theta_{n,m}, \phi_{n,m}) G_{r_n}(\theta_{n,m}, -\phi_{n,m})} \frac{e^{-j(kR_{n,m} - \beta_m)}}{R_{n,m}} \right|^2 \quad (3)$$

The total transmitted power (P_T) radiated by the transmitting array can be expressed as $\sum_{m=1}^{N_t} P_{t_m}$. Finally, the PTE of the Rx array can be expressed by

$$PTE = \frac{P_R}{P_T} = \frac{\left(\frac{\lambda}{4\pi}\right)^2 \sum_{n=1}^{N_r} \left| \sum_{m=1}^{N_t} \sqrt{P_{t_m} G_{t_m}(\theta_{n,m}, \phi_{n,m}) G_{r_n}(\theta_{n,m}, -\phi_{n,m})} \frac{e^{-j(kR_{n,m} - \beta_m)}}{R_{n,m}} \right|^2}{\sum_{m=1}^{N_t} P_{t_m}} \quad (4)$$

It is known that $G_{t_m}(\theta_{n,m}, \phi_{n,m})$, $G_{r_n}(\theta_{n,m}, -\phi_{n,m})$, and $R_{n,m}$ are related to the layout of the receiving antenna array elements. From Eq. (4), it can be seen that under the condition that the transmitting array is unchanged, the PTE can be improved by reasonably adjusting the number of receiving array elements and optimizing the layout of receiving array elements.

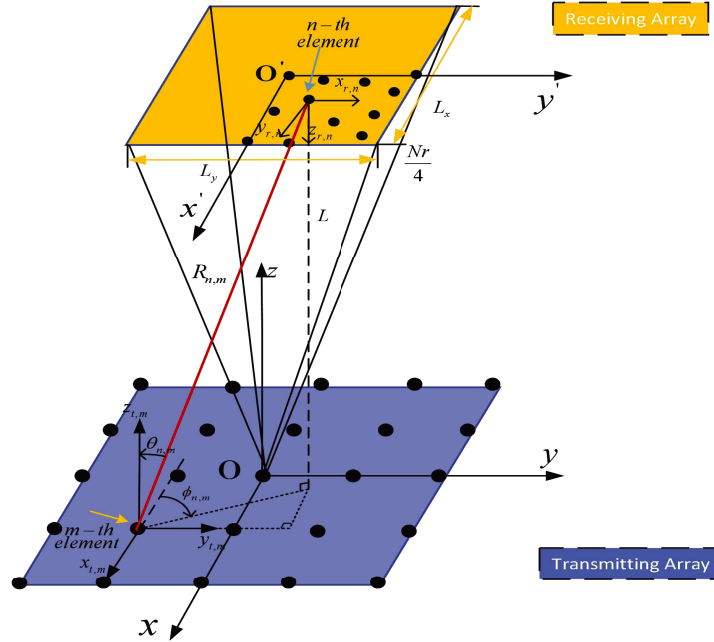


Figure 1. Geometry of the MPT system.

3. SYNTHESIS METHOD OF THE SRPRA

As described in Section 2, designing an optimal SRPRA can be reduced to a multi-constrained optimization problem, i.e., finding the optimal received power by optimizing the locations of the receiving array elements to maximize the PTE while satisfying the minimum array element spacing and keeping the array aperture size constant. In this paper, we solve the optimal synthesis of the SRPRA for maximizing the PTE by the following two subsections.

3.1. Establishment of the SRPRA Model

In the first subsection, since the array elements at symmetrical locations receive the same power, it is possible to share a feeding network to reduce system cost and simplify the design process. Therefore, we distribute the positions of the receiving array elements symmetrically around the center, that is, only the coordinates of the array elements in the first quadrant need to be determined, then the coordinates

of the other three quadrants can be obtained. We set the number of receiving array elements Nr as a multiple of 4, and there are $Nr/4$ elements in each quadrant. Therefore, based on the analysis of the above constraints, the corresponding optimization model can be developed as

$$\left\{ \begin{array}{l} \text{find } [\mathbf{X}, \mathbf{Y}, \mathbf{Z}] = [x_{r,1}, x_{r,2}, \dots, x_{r,Nr}, y_{r,1}, y_{r,2}, \dots, y_{r,Nr}, z_{r,1}, z_{r,2}, \dots, z_{r,Nr}] \\ \text{maximize } PTE([\mathbf{X}, \mathbf{Y}, \mathbf{Z}]) \\ \text{subject to (a) } z_{r,i} = L, \quad i = \{1, 2, \dots, Nr\}; \\ \quad \text{(b) } (x_{r,n}, y_{r,n}) = (-x_{r,n-Nr/4}, y_{r,n-Nr/4}), \quad n = \{(Nr/4) + 1, \dots, Nr/2\}; \\ \quad \text{(c) } (x_{r,n}, y_{r,n}) = (-x_{r,n-Nr/2}, -y_{r,n-Nr/2}), \quad n = \{(Nr/2) + 1, \dots, 3Nr/4\}; \\ \quad \text{(d) } (x_{r,n}, y_{r,n}) = (x_{r,n-3Nr/4}, -y_{r,n-3Nr/4}), \quad n = \{(3Nr/4) + 1, \dots, Nr\}; \\ \quad \text{(e) } d_{\min}/2 \leq x_{r,n} \leq L_x/2, \quad n = \{1, 2, \dots, Nr/4\}; \\ \quad \text{(f) } d_{\min}/2 \leq y_{r,n} \leq L_y/2, \quad n = \{1, 2, \dots, Nr/4\}; \\ \quad \text{(g) } \sqrt{(x_{r,i} - x_{r,j})^2 + (y_{r,i} - y_{r,j})^2} \geq d_{\min} \quad i, j = \{1, 2, \dots, Nr/4\}, \quad i \neq j; \\ \quad \text{(h) } (x_{r,Nr/4}, y_{r,Nr/4}) = (L_x/2, L_y/2) \end{array} \right. \quad (5)$$

where $[\mathbf{X}, \mathbf{Y}, \mathbf{Z}]$ is the coordinate vector of the receiving array elements and the optimization variable of the SRPRA model. The optimization objective is to maximize the PTE . In this model, since the distance L between two arrays is fixed, the \mathbf{Z} -coordinates of the receiving array elements can be expressed by the constraint (a) in Eq. (5). In this case, only the two-dimensional vector $[\mathbf{X}', \mathbf{Y}']$ needs to be optimized, reducing the complexity of optimization. In addition, to ensure that the aperture size is $L_x \times L_y$, the condition (h) must be satisfied, which in turn requires that we know the coordinates of the four corner points. Therefore, the above model can be simplified as

$$\left\{ \begin{array}{l} \text{find } [\mathbf{X}', \mathbf{Y}'] = [x_{r,1}, x_{r,2}, \dots, x_{r,(Nr/4)-1}, y_{r,1}, y_{r,2}, \dots, y_{r,(Nr/4)-1}] \\ \text{maximize } PTE([\mathbf{X}', \mathbf{Y}']) \\ \text{subject to (a) } (x_{r,n}, y_{r,n}) = (-x_{r,n-Nr/4}, y_{r,n-Nr/4}), \quad n = \{(Nr/4) + 1, \dots, (Nr/2) - 1\}; \\ \quad \text{(b) } (x_{r,n}, y_{r,n}) = (-x_{r,n-Nr/2}, -y_{r,n-Nr/2}), \quad n = \{(Nr/2) + 1, \dots, (3Nr/4) - 1\}; \\ \quad \text{(c) } (x_{r,n}, y_{r,n}) = (x_{r,n-3Nr/4}, -y_{r,n-3Nr/4}), \quad n = \{(3Nr/4) + 1, \dots, Nr - 1\}; \\ \quad \text{(d) } d_{\min}/2 \leq x_{r,n} < L_x/2, \quad n = \{1, 2, \dots, (Nr/4) - 1\}; \\ \quad \text{(e) } d_{\min}/2 \leq y_{r,n} < L_y/2, \quad n = \{1, 2, \dots, (Nr/4) - 1\}; \\ \quad \text{(f) } \sqrt{(x_{r,i} - x_{r,j})^2 + (y_{r,i} - y_{r,j})^2} \geq d_{\min} \quad i, j = \{1, 2, \dots, (Nr/4) - 1\}, \quad i \neq j; \end{array} \right. \quad (6)$$

The optimization process of this model can be roughly described as follows: firstly, the location coordinates of the initial receiving array elements are randomly distributed in the first quadrant under the constraints (d), (e), and (f) in Eq. (6). Secondly, the coordinates of the remaining three quadrants can be obtained according to the symmetry relationships of the array elements in the four quadrants described by (a), (b), and (c) in Eq. (6). Finally, according to Eq. (4), the PTE can be calculated, and then by continuously optimizing the positions of the array elements, the maximum PTE and the optimal array element layout of the SRPRA can be obtained.

3.2. Proposal of the IACPSO Algorithm

In the second subsection, the IACPSO algorithm is proposed in view of the fact that the population diversity of the SPSO algorithm decreases in the late iterations, and the SPSO algorithm is prone to fall into local optimization and premature convergence [20–23]. The innovation of the IACPSO algorithm is to propose a novel strategy for adaptively adjusting the inertia weights and learning factors according to the degree of population prematureness and the fitness values of the particles [24]. Different adaptive operations are applied to different particles, so that the population always maintains the diversity of inertia weights, and the learning factors also change dynamically with the increase of iterations. As a result, the IACPSO algorithm not only has a fast convergence speed and good stability, but also improves the search efficiency and makes it easier to obtain the optimal solution.

According to [25], the logistic mapping mathematical expression in this algorithm is defined as

$$z_{k+1} = \mu z_k(1 - z_k) \quad z_k \in [0, 1] \quad (7)$$

where $\mu \in [0, 4]$ is called the control variable. In the proposed IACPSO algorithm, let $\mu = 4$ and Eq. (7) is in a fully chaotic state. Then, the velocity and position of particles are initialized by the logistic mapping based on randomness and ergodicity. As a result, the quality of the initial solution is improved, and the global search capability of this algorithm is enhanced.

The index in [26] is cited to measure the degree of premature convergence of the particle swarm, which can be expressed as

$$\Delta(t) = |f_g(t) - f_{ap}(t)| \quad (8)$$

where $f_g(t)$ is the fitness value of the global optimal particle, and $f_{ap}(t)$ is the average fitness value of particles whose $f_i(t) > f_{av}(t)$, where $f_i(t)$ is the fitness value of the i -th particle in the t -th iteration, and $f_{av}(t)$ is the average fitness value of all particles. $\Delta(t)$ can be used to measure the degree of early convergence of the particle swarm; the smaller the $\Delta(t)$ is, the more the swarm tends to converge early.

The adaptive inertia weight adjustment strategy for the particles with the fitness value $f_i(t)$ is as follows.

Step 1: For the particles whose $f_i(t) \geq f_{ap}(t)$, their inertia weights ($w_i(t)$) need to be taken as small values to enhance the ability to find the optimal solution locally, which can be adaptively adjusted as

$$w_i(t) = w_s - (w_s - w_{\min}) \left| \frac{f_i(t) - f_{ap}(t)}{\Delta(t)} \right| \quad (9)$$

where $w_s = (w_{\min} + w_{\max})/2$ is the middle value of the range of $w_i(t)$, and w_{\min} and w_{\max} are the minimum value and maximum value of $w_i(t)$, respectively.

Step 2: For the particles whose $f_{aw}(t) \leq f_i(t) < f_{ap}(t)$, where $f_{aw}(t)$ is the average fitness value of particles whose $f_i(t) < f_{av}(t)$, their inertia weights can be adaptively adjusted according to a nonlinear decreasing strategy, which can be expressed as [24]

$$w_i(t) = (w_{\max} + w_{\min})/2 + \tanh(-4 + 8 \times (T - t)/T) \times (w_{\max} - w_{\min})/2 \quad (10)$$

where $\tanh(\cdot)$ is the hyperbolic tangent function, and T is the maximum number of iterations.

Step 3: For the particles whose $f_i(t) < f_{aw}(t)$, their inertia weights ($w_i(t)$) need to be taken as large values to enhance the ability to find the optimal solution globally, which can be adaptively adjusted as

$$w_i(t) = 1.5 - \frac{1}{1 + k_1 \exp \left[\left(-10k_2 \left(\frac{\Delta(t) \cdot 2t}{T} - 1 \right) \right) \right]} \quad (11)$$

The parameter k_1 is used to control the upper limit of $w_i(t)$; k_2 is the damping coefficient, which is used to control the regulation ability of $w_i(t)$ and generally taken as $[0, 1]$.

In addition, an adaptive learning factors adjustment strategy is proposed for the early convergence phenomenon of the population to improve the ability of the algorithm to find the optimal solution globally. The mathematical description of the strategy can be written as

$$\begin{cases} c_{i1}(t) = c_{1\max} - (c_{1\max} - c_{1\min}) \left| \frac{f_i(t) - f_{ip}(t)}{f_{ip}(t)} \right| \\ c_{i2}(t) = c_{2\min} + (c_{2\max} - c_{1\min}) \left| \frac{f_i(t) - f_g(t)}{f_g(t)} \right| \end{cases} \quad (12)$$

where $f_{ip}(t)$ is the optimal fitness value of the i -th particle. $c_{1\max}$ and $c_{1\min}$ are the maximum and minimum values of the individual learning factors, respectively. $c_{2\max}$ and $c_{2\min}$ are the maximum and minimum values of the social learning factors, respectively.

Therefore, the IACPSO algorithm designed in this paper updates the velocity and position of particles which can be expressed as

$$\begin{cases} v_i(t+1) = w_i(t) \times v_i(t) + c_{i1}(t) \times rand \times (p_i(t) - x_i(t)) + c_{i2}(t) \times rand \times (g(t) - x_i(t)) \\ x_i(t+1) = x_i(t) + v_i(t+1) \end{cases} \quad (13)$$

where $i = 1, 2, \dots, N$, N is the number of particles, $p_i(t)$ the local optimal value of the i -th particle, $g(t)$ the global optimal value, and the *rand* the random number between $(0, 1)$.

4. SIMULATION EXPERIMENT AND NUMERICAL RESULTS ANALYSIS

In this section, we discuss the synthesis results from the following three aspects. Firstly, the IACPSO algorithm proposed in this paper synthesizes the SRPRA with different parameters and analyzes the corresponding synthesis results. Secondly, to verify the performance of the SRPRA, the synthesis results of the SRPRA are compared with those of the SRCAA presented in [17] under the same parameters. Finally, we compare the IACPSO algorithm with the SPSO algorithm to demonstrate the advantages of the IACPSO algorithm in the SRPRA synthesis. The CPU adopted for all simulations is AMD Core R5-5600H at 3.3 GHz with 16 GB RAM, and the numerical analysis software is MATLAB R2019a.

To facilitate later comparison of the results, we introduce two evaluation indicators. One is the sparse ratio γ , which is defined as the ratio of the number of elements (Nr) used by the SRPRA to the number of elements (N_f) used by the fully populated receiving array for the same aperture size and can be expressed as

$$\gamma = \frac{Nr}{N_f}, \quad N_f = \left(\frac{L_x}{d_{\min}} + 1 \right) \times \left(\frac{L_y}{d_{\min}} + 1 \right) \quad (14)$$

The other is the sidelobe level outside the receiving area (CSL), which is defined as the ratio of the maximum power level outside the receiving area Ψ to the maximum power level in the entire visible area Ω . According to [27], CSL (dB) can be written as

$$CSL(\text{dB}) = 10 \lg \frac{\max_{u,v \notin \Psi} |F(u,v)|^2}{\max_{u,v \in \Omega} |F(u,v)|^2} \quad (15)$$

where $\Psi \triangleq \{(u,v) : -u_0 \leq u \leq u_0, -v_0 \leq v \leq v_0\}$ and $\Omega \triangleq \{u,v : u^2 + v^2 \leq 1\}$.

According to [27], the rectangular receiving array factor can be expressed as

$$F(u,v) = \sum_{i=1}^{Nr} P_{r_n} e^{ik(ux_{r,n} + vy_{r,n})} \quad (16)$$

where $u = \sin \theta \cos \varphi$ and $v = \sin \theta \sin \varphi$ are direction parameters; θ and φ are the elevation angle and azimuth angle, respectively.

Since the focus of this paper is on the Rx array, and the Tx array is not relevant to our research objectives, the parameters of the Tx array in all simulation experiments in this section are the same as those in [16]; $Nt = 8 \times 8$ array elements are uniformly distributed in the XOY plane; the minimum Tx array element spacing is $d_{\min} = 0.5\lambda$. The relative distance L between the Tx and Rx arrays is 4λ . In this paper, we set the operating frequency to 2.45 GHz and normalize the wavelength to 1. Fig. 2(a)

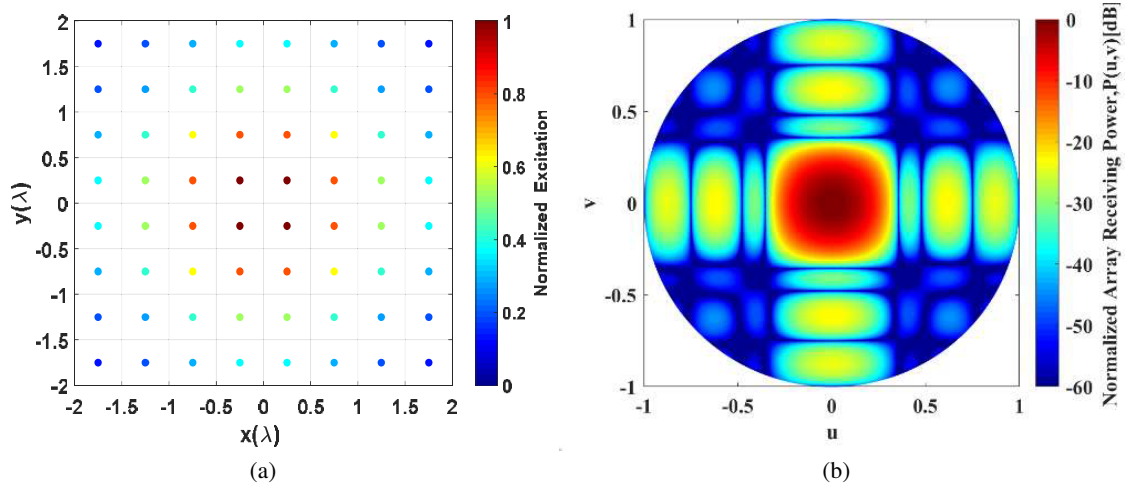


Figure 2. Synthesis results of the Tx array (a) layout and weight, (b) radiation power.

shows the positions and excitation of the Tx elements, i.e., the excited power-set (P_{t_m}) when applying -18 dB Taylor weighting to reduce the side-lobe, and Fig. 2(b) shows a map of the radiation power direction of the transmitting array located in the XOY plane.

4.1. Influence of Different Parameters on Synthesis Results

The number of array elements N_r determines the PTE of the SRPRA to some extent. We investigate the effects of the number of array elements on synthesis results of the SRPRA and the traditional uniform receiving array (TURA) in the first experiment. In this experiment, we select the SRPRA and TURA with an aperture size of $L_x \times L_y = 4.5\lambda \times 4.5\lambda$, and at this aperture, the full array consists of 100 elements. Finally, the synthesis results are shown in Table 1.

Table 1. Synthesis results of the SRPRA and the TURA.

SRPRA			TURA			γ (%)
N_r	PTE (%)	CSL (dB)	N_s	PTE (%)	CSL (dB)	
48	42.53	-9.83	48	36.62	-10.89	48
40	40.74	-8.27	40	32.89	-9.01	40
32	36.66	-7.04	32	28.87	-8.24	32
24	31.29	-6.45	24	26.21	-7.19	24
16	28.90	-5.99	16	19.31	-4.93	16

In Table 1, N_r and N_s represent the number of elements used by the SRPRA and TURA, respectively. Analyzing the synthesis results in the table, we can draw the following conclusions: (I) In the same aperture, the more the number of elements of the two receiving arrays is, the higher the PTE , and the lower CSL are. (II) When the number of array elements is the same, the SRPRA has higher PTE and lower CSL than the TURA (e.g., $[PTE, CSL]_{N_r=24} = [31.29\%, -6.45 \text{ dB}]$ vs. $[PTE, CSL]_{N_s=24} = [26.21\%, -7.19 \text{ dB}]$ and $[PTE, CSL]_{N_r=40} = [40.74\%, -8.27 \text{ dB}]$ vs. $[PTE, CSL]_{N_s=40} = [32.89\%, -9.01 \text{ dB}]$). (III) When the number of array elements is different, the SRPRA can use fewer elements to obtain higher PTE (e.g., $[PTE, CSL]_{N_r=40} = [40.74\%, -8.27 \text{ dB}]$ vs. $[PTE, CSL]_{N_s=48} = [36.62\%, -10.89 \text{ dB}]$, the array element position distribution and array received power of the SRPRA are shown in Fig. 3). Compared with the TURA, the SRPRA saves 8 elements, and PTE is 4.12% higher, but CSL is increased by 2.62 dB when $N_r = 40$ and $N_s = 48$. This is acceptable for the

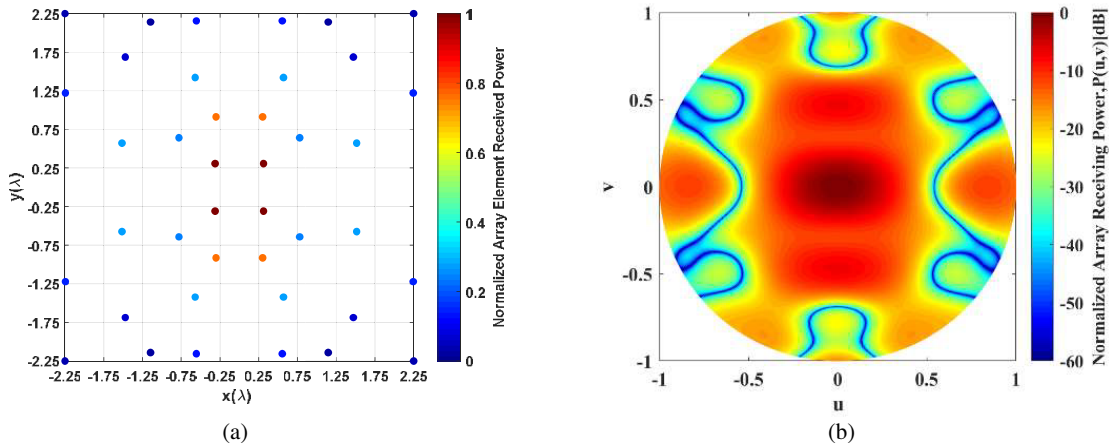


Figure 3. Synthesis results of the SRPRA ($N_r = 40$) (a) layout and received power, (b) receiving power.

MPT system that values efficiency.

Next, we discuss the effects of different minimum element spacings (d_{\min}) on the results of the SRPRA synthesis for the same array aperture and number of array elements. We set up three different types of the SRPRA with the number of array elements $Nr = 20$ and the array aperture $L_x \times L_y = 4.5\lambda \times 4.5\lambda$; the number of array elements $Nr = 100$ and the array aperture $L_x \times L_y = 9.5\lambda \times 9.5\lambda$; and the number of array elements $Nr = 260$ and the array aperture $L_x \times L_y = 14.5\lambda \times 14.5\lambda$, respectively. Fig. 4 shows the synthesis results from a series of experiments conducted at different array element spacings $d_{\min} \in \{0.5\lambda, 0.52\lambda, \dots, 0.7\lambda\}$.

According to Fig. 4, we can draw the following conclusions through comparison: (I) For the same array aperture size, the *PTE* of the SRPRA model decreases with increasing d_{\min} , and the larger the array aperture is, the more significantly the *PTE* decreases. The reason for this rule is that the received power density in the center of the array is large, so the large array element density in the center region (i.e., small spacing) helps to increase the *PTE*. If the minimum spacing d_{\min} is large, it makes the array element density in the center region small (i.e., large spacing), which results in a small *PTE*. (II) Similarly, the *CSL* decreases with increasing d_{\min} . In addition, the *CSL* shows different degrees of decrease with increasing d_{\min} in different sizes of array apertures (e.g., when the array aperture is $L_x \times L_y = 9.5\lambda \times 9.5\lambda$ and the d_{\min} takes the values of 0.5λ , 0.6λ and 0.7λ in turn, the synthesis results are $[PTE, CSL] |_{d_{\min}=0.5} = [40.96\%, -9.69 \text{ dB}]$ vs. $[PTE, CSL] |_{d_{\min}=0.6} = [30.03\%, -10.68 \text{ dB}]$ vs. $[PTE, CSL] |_{d_{\min}=0.7} = [29.57\%, -12.11 \text{ dB}]$, and their the array element position distribution and array received power of the SRPRA are shown in Fig. 5, Fig. 6 and Fig. 7).

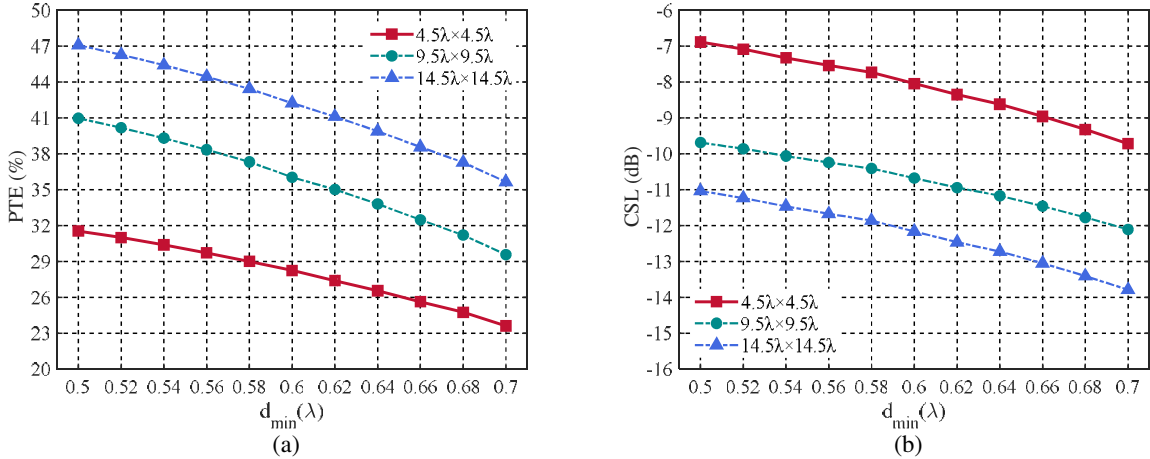


Figure 4. Synthesis results of the SRPRA with different minimum element spacings (a) *PTE*, (b) *CSL*.

Finally, we explore the relationship between the *PTE* and the number of array elements Nr with the variation of array aperture Dr ($Dr = L_x = L_y$). Fig. 8 shows the synthesis results from a set of experiments at different apertures $Dr \in \{4\lambda, 5\lambda, \dots, 15\lambda\}$. From Fig. 8, it can be observed that when $Dr \leq 10\lambda$, the value of the *PTE* increases significantly with Dr , while Nr increases slowly. When $Dr > 10\lambda$, as the Dr continues to increase, the number of elements Nr increases significantly, but the *PTE* starts to slowly increase.

As a result, the optimal array aperture Dr_{opt} for the SRPRA is equal to 10λ , and the array element position distribution and array received power of the SRPRA are shown in Fig. 9.

4.2. Comparison of the SRPRA and the SRCAA

In order to demonstrate the advantages of the SRPRA in the MPT system, we compare its synthesis results with those of the SRCAA in [17]. To compare the synthesis performance of the SRPRA and the SRCAA, the values of L and d_{\min} are the same as those in [17]. Then the synthesis results of the

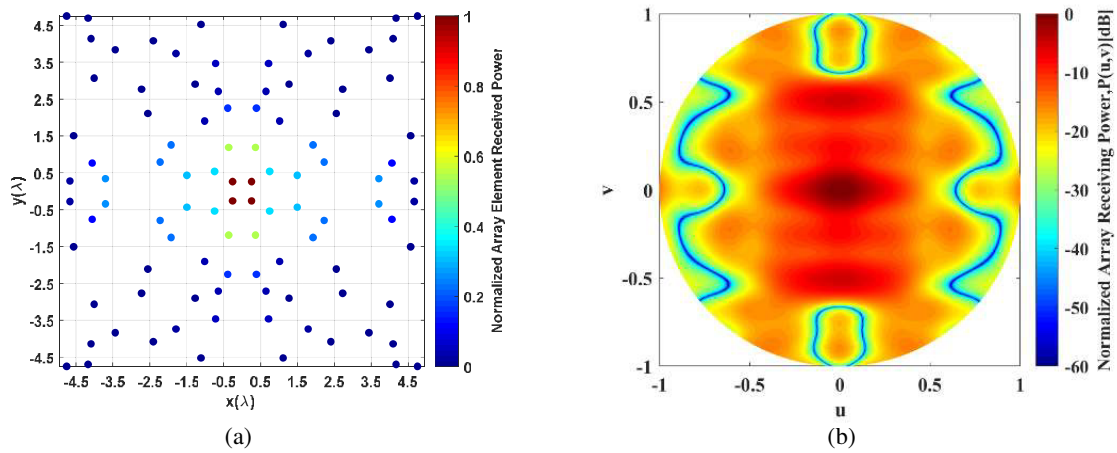


Figure 5. Synthesis results of the SRPRA ($d_{\min} = 0.5\lambda$) (a) layout and received power, (b) receiving power.

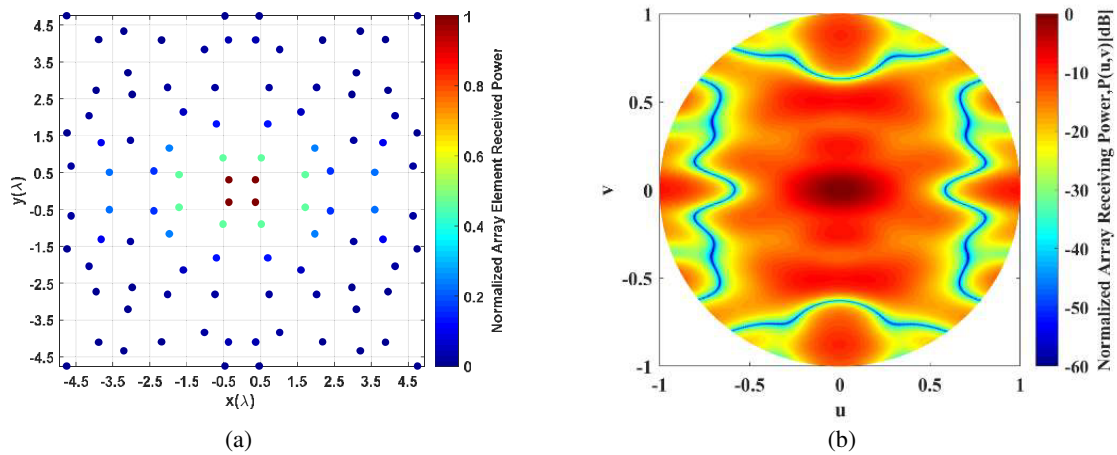


Figure 6. Synthesis results of the SRPRA ($d_{\min} = 0.6\lambda$) (a) layout and received power, (b) receiving power.

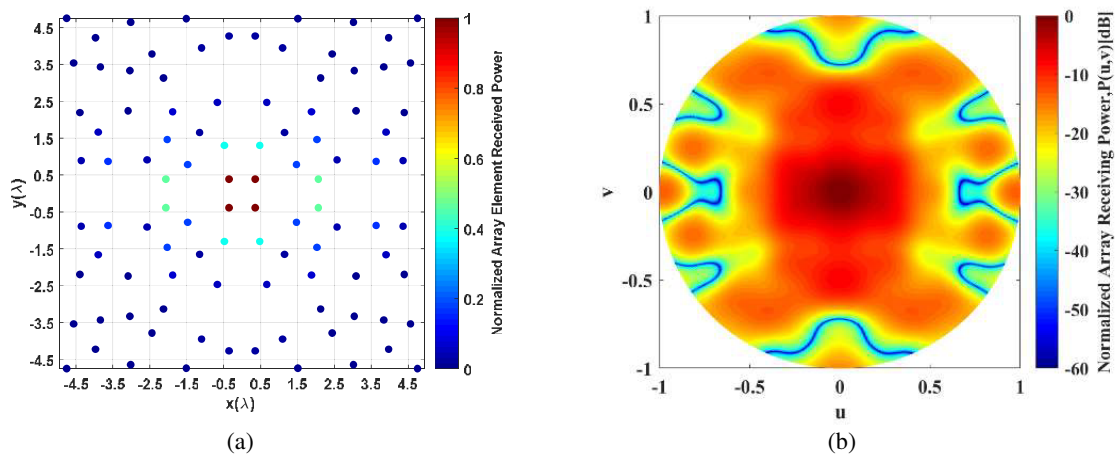


Figure 7. Synthesis results of the SRPRA ($d_{\min} = 0.7\lambda$) (a) layout and received power, (b) receiving power.

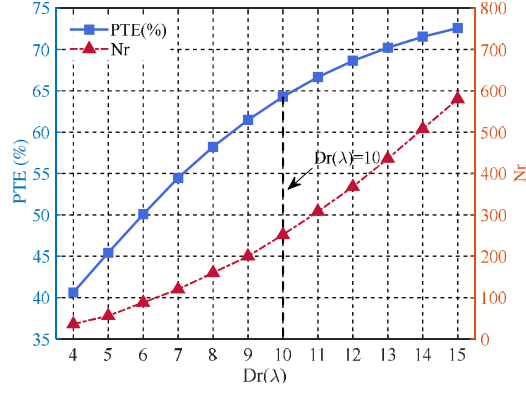


Figure 8. Behavior of the PTE of the SRPRA versus the aperture Dr and the number of elements N_r .

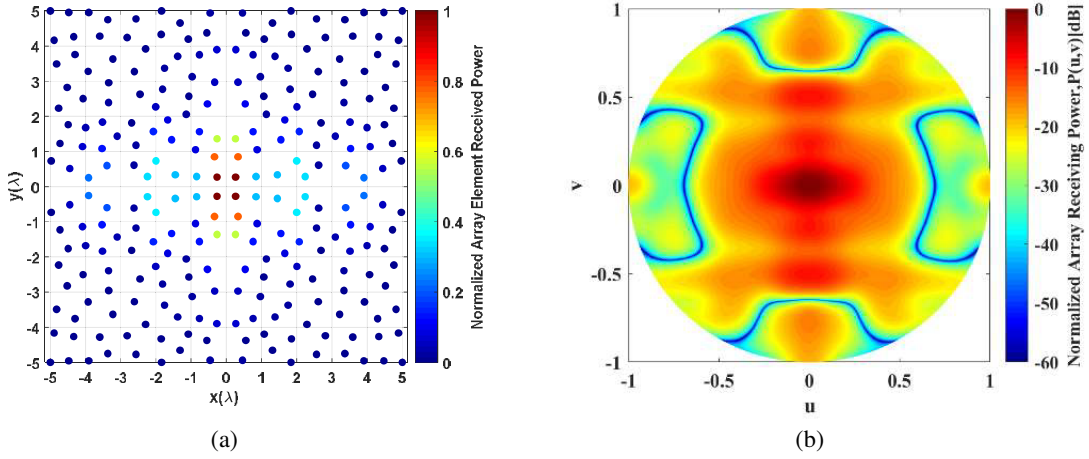


Figure 9. Synthesis results of the SRPRA ($Dr = 10\lambda$) (a) layout and received power, (b) receiving power.

two receiving arrays are listed in Table 2. Fig. 10 shows the synthesis results of a set of comparative experiments performed with the SRPRA and the SRCAA at different apertures $Dr \in \{4\lambda, 5\lambda, \dots, 15\lambda\}$.

Table 2. Comparison of synthesis results between the SRPRA and the SRCAA.

		SRPRA			SRCAA				
$L_x = L_y (\lambda)$	N_r	$PTE (\%)$	$CSL (dB)$	$\gamma (\%)$	$Dr (\lambda)$	N_r	$PTE (\%)$	$CSL (dB)$	$\gamma (\%)$
5	40	38.84	-7.44	33.06	5	40	34.26	-6.51	43.01
	44	42.17	-8.18	39.67		48	37.26	-6.78	51.61
	48	45.21	-8.77	49.59		56	40.45	-7.26	60.21
10	180	49.22	-12.70	40.82	10	160	44.85	-9.68	46.92
	200	53.18	-13.13	45.35		180	48.30	-10.04	52.79
	220	56.40	-13.57	49.89		200	51.55	-11.27	58.65
15	460	64.14	-19.28	47.87	15	460	58.19	-15.34	61.58
	480	67.11	-20.21	49.95		480	60.25	-15.64	64.26
	500	69.56	-21.06	52.03		500	62.49	-16.44	66.93

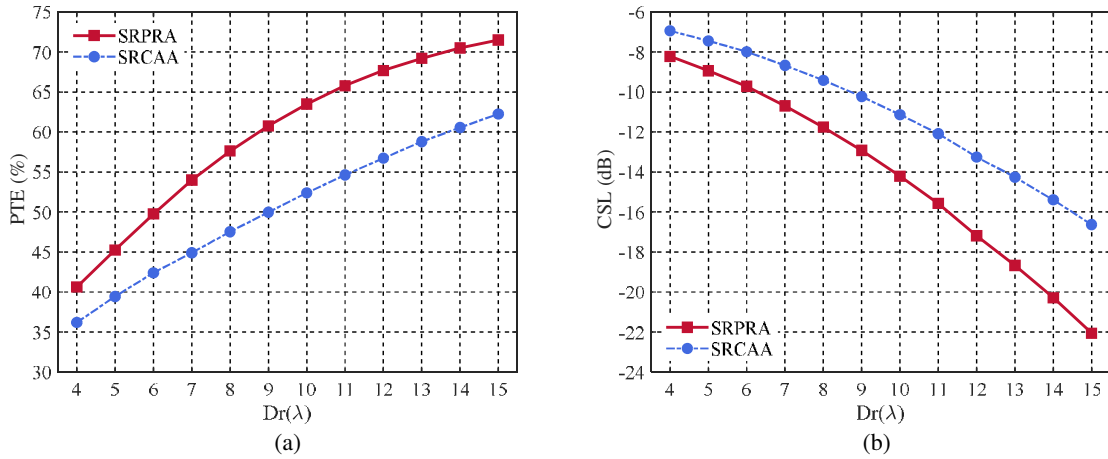


Figure 10. Synthesis results of the SRPRA and the SRCAA at different apertures (a) PTE , (b) CSL .

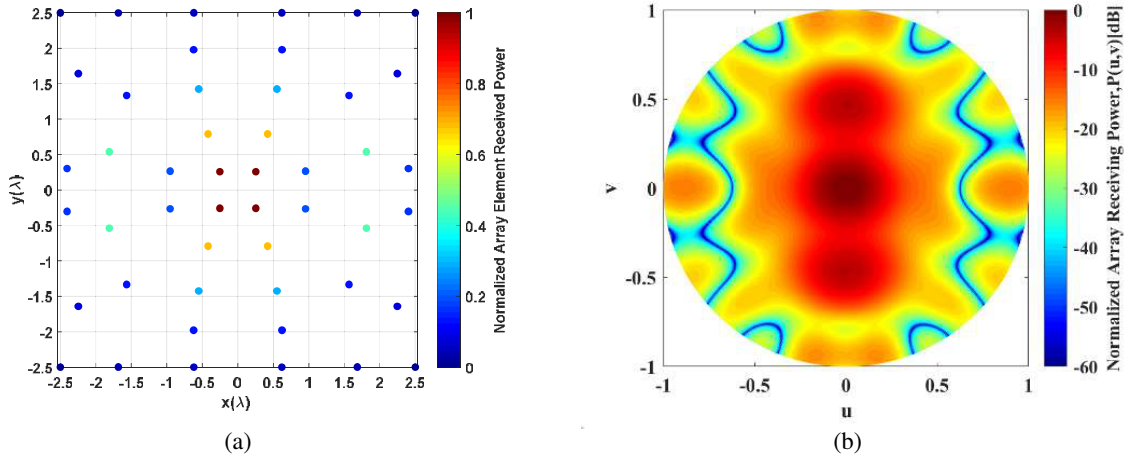


Figure 11. Synthesis results of the SRPRA ($Dr = 5\lambda$ and $Nr = 48$) (a) layout and received power, (b) receiving power.

Comparing the performance parameters of the SRPRA (including PTE , CSL , and γ) with those of the SRCAA, the synthesis performance of the SRPRA is significantly improved. Obviously, we observed that the SRPRA can use fewer elements to obtain higher PTE and lower CSL with the same array aperture, and the γ of the array can also be smaller (e.g., when $Dr = 5\lambda$, the synthesis results are $[PTE, CSL, \gamma] |_{Nr=48} = [45.21\%, -8.77 \text{ dB}, 45.59\%]$ and $[PTE, CSL, \gamma] |_{Nr=56} = [40.45\%, -7.26 \text{ dB}, 60.21\%]$, respectively.) As a result, the SRPRA saves 14.29% elements and has 4.76% higher PTE and 1.51 dB lower CSL than the SRCAA. Fig. 11 and Fig. 12 show the array element position distribution and array received power for the SRPRA and SRCAA when $Dr = 5\lambda$ and $Nr = 48$, respectively.

Some conclusions can be drawn from Table 2 and Fig. 10: (I) Obviously, with the increase of the array aperture size, the PTE of the two receiving arrays can be higher, and the CSL can be lower. (II) Compared to the SRCAA, the SRPRA has 7.07% higher PTE and 4.62 dB lower CSL when $L_x \times L_y = 15\lambda \times 15\lambda$ and $Nr = 500$. Therefore, the SRPRA has more significant performance under the same aperture and array elements. (III) Comparing Fig. 11(a) and Fig. 12(a), it can be clearly observed that each array element within the SRCAA is randomly distributed and has different received powers, which greatly increases the complexity of the feeding network. However, for the SRPRA, the received powers of the array elements are equal at symmetrical positions, which not only simplifies the feeding circuit, but also reduces the cost of the MPT system.

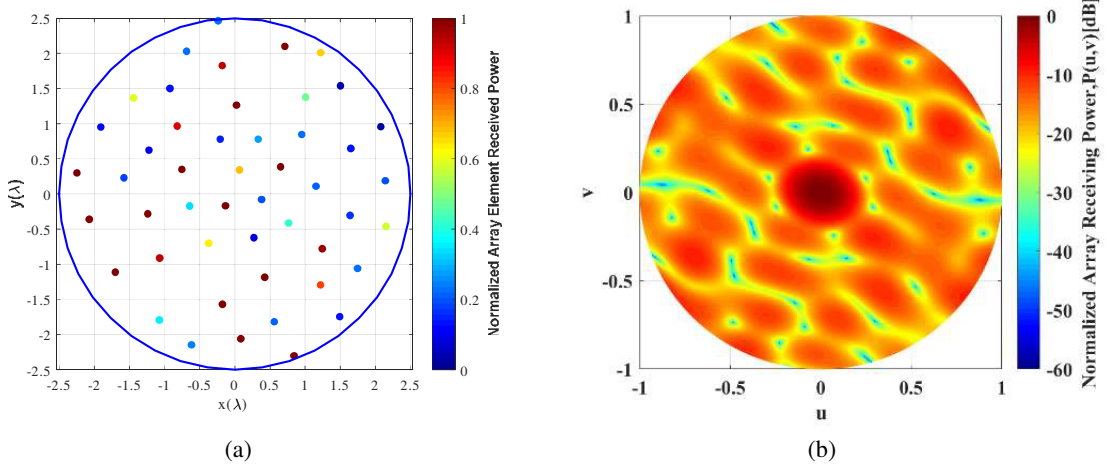


Figure 12. Synthesis results of the SRCAA ($Dr = 5\lambda$ and $Nr = 48$) (a) layout and received power, (b) receiving power.

In summary, the synthesis performance of the SRPRA is better than that of the SRCAA, which verifies the validity of the SRPRA model proposed in this paper.

4.3. Performance of the IACPSO Algorithm

At the end of this section, to verify the stability and efficiency of the proposed IACPSO algorithm in the SRPRA synthesis, we compare it with the SPSO algorithm. It needs to be noted that in this comparison experiment, the parameters and steps are the same except that two different optimization algorithms are used in the synthesis algorithm. The number of optimization iterations is set to 200.

Firstly, we select three different apertures of the SRPRA model for algorithm optimization. The aperture of the first array is $L_x \times L_y = 4.5\lambda \times 4.5\lambda$, and the number of elements is $Nr = 44$; the aperture of the second array is $L_x \times L_y = 9.5\lambda \times 9.5\lambda$, and the number of elements is $Nr = 228$; the aperture of the third array is $L_x \times L_y = 14.5\lambda \times 14.5\lambda$, and the number of elements is $Nr = 548$. Fig. 13(a) shows the fitness curves of six optimizations when the two algorithms optimize three different sizes of apertures.

Secondly, when $L_x \times L_y = 9.5\lambda \times 9.5\lambda$, the two algorithms are repeated to optimize the experiment three times, and the fitness curves are shown in Fig. 13(b).

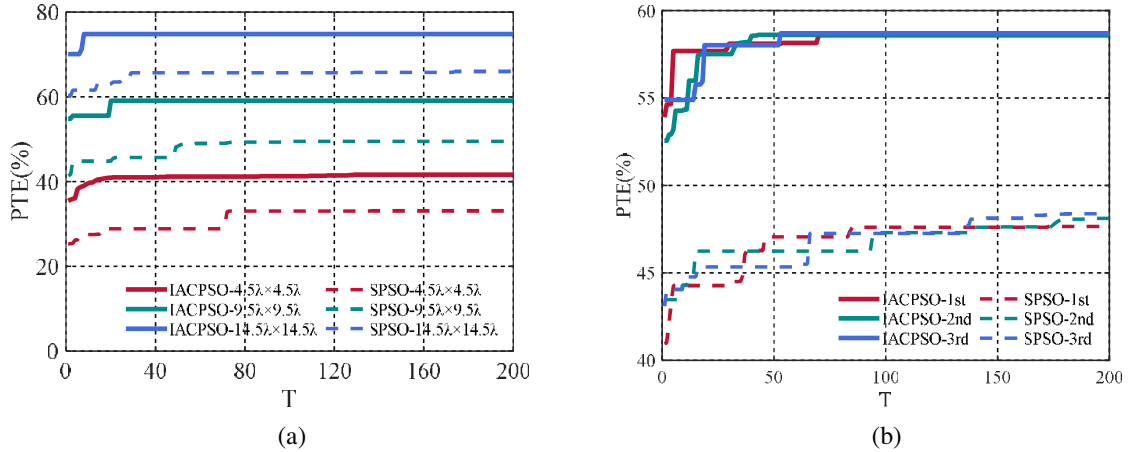


Figure 13. Comparison of the IACPSO algorithm and the SPSO algorithm (a) fitness variation curves, (b) three repeated optimizations of two algorithms.

As can be seen from Fig. 13(a), the IACPSO algorithm has a higher fitness value after stabilization than the SPSO algorithm, and thus the better PTE can be obtained, which proves that the IACPSO algorithm has a more efficient performance in dealing with the SRPRA synthesis problem. In addition, the optimization curves show that the IACPSO algorithm stabilizes at about 20 iterations, so the convergence speed is significantly faster than that of the SPSO algorithm. As can be seen from Fig. 13(b), the three times optimization curves of the IACPSO algorithm almost coincide after about 70 generations, so the IACPSO algorithm is more stable than the SPSO algorithm.

To sum up, since the IACPSO algorithm adopts a new optimization mechanism and update strategy, it can avoid the SPSO algorithm from falling into local optimization during the optimization process and thus obtain a better global solution, which verifies that the IACPSO algorithm has the advantages of stability and efficiency in the SRPRA synthesis.

5. CONCLUSION

In this paper, we propose a sparse model of the rectangular aperture array, which is SRPRA, for MPT system. After deriving the PTE of the SRPRA, we propose IACPSO algorithm based on a novel optimization strategy to maximize the PTE for the SRPRA. Under the constraints of array aperture and minimum array element spacing, the PTE can be improved by reasonably adjusting the number of receiving array elements and optimizing the layout of receiving array elements.

In addition, we conduct extensive simulation experiments to verify the advantages of the proposed SRPRA model and the effectiveness of the synthesis method. Firstly, we discuss the effects of the number of array elements, minimum array element spacing, and array aperture size on the synthesis results. Secondly, to demonstrate the advantages of the SRPRA model in the MPT system, we compare the synthesis results of the SRPRA with those of the SRCAA in [17]. After analyzing the synthesis results, it was found that the SRPRA can achieve higher PTE and lower CSL with fewer elements and has a simpler feeding network than the SRCAA. Finally, to verify that the proposed IACPSO algorithm has excellent performance in optimizing the SRPRA model, we compare it with the SPSO algorithm. As a result, the synthesis results show that the IACPSO algorithm converges faster and achieves higher PTE for three different array apertures, and the fitness curves obtained by repeating the optimization three times for the same array aperture can largely overlap. Therefore, the IACPSO algorithm has a more stable and efficient performance.

ACKNOWLEDGMENT

This work was supported by the National Natural Science Foundation of China (Grant No. 51877151) and the Program for Innovative Research Team in University of Tianjin (Grant No. TD13-5040).

REFERENCES

1. Nakamoto, Y., N. Hasegawa, Y. Takagi, et al., "A study on microwave power transfer to rectangular antenna for stratospheric platform," *2019 IEEE Asia-Pacific Microwave Conference (APMC)*, 996–998, 2019.
2. Hui, Q., K. Jin, and X. Zhu, "Directional radiation technique for maximum receiving power in microwave power transmission system," *IEEE Transactions on Industrial Electronics*, Vol. 67, No. 8, 6376–6386, 2020.
3. Matsumoto, H., "Space solar power station (SSPS) and microwave power transmission (WPT)," *IEEE Topical Conference on Wireless Communication Technology*, 6, Kyoto, Japan, November 2003.
4. Sasaki, S., K. Tanaka, and K. Maki, "Microwave power transmission technologies for solar power satellites," *Proceedings of the IEEE*, Vol. 101, No. 6, 1438–1447, 2013.
5. Li, J., J. Pan, and X. Li, "A novel synthesis method of sparse nonuniform-amplitude concentric ring arrays for microwave power transmission," *Progress In Electromagnetics Research C*, Vol. 107, 1–15, 2021.

6. Massa, A., G. Oliveri, F. Viani, and P. Rocca, "Array designs for long-distance wireless power transmission: State-of-the-art and innovative solutions," *Proceedings of the IEEE*, Vol. 101, No. 6, 1464–1481, 2013.
7. Takahashi, T., T. Sasaki, Y. Homma, et al., "Phased array system for high efficiency and high accuracy microwave power transmission," *IEEE International Symposium on Phased Array Systems & Technology*, 1–7, Waltham, MA, January 2017.
8. Gavan, J. and S. Tapuch, "Microwave wireless-power transmission to high-altitude-platform systems," *Radio Sci. Bull.*, Vol. 83, No. 3, 25–42, 2017.
9. Shinohara, N., "Wireless power transfer in Japan: Regulations and activities," *2020 14th European Conference on Antennas and Propagation (EuCAP)*, 1–4, 2020.
10. Qiang, C., C. Xing, and F. Pan, "A comparative study of space transmission efficiency for the microwave wireless power transmission," *2015 IEEE Asia-Pacific Microwave Conference (APMC)*, 1–3, Nanjing, China, December 2016.
11. Nepa, P. and A. Buffi, "Near-field-focused microwave antennas: Near-field shaping and implementation," *IEEE Antennas and Propagation Magazine*, Vol. 59, No. 3, 42–53, 2017.
12. Li, X., K. M. Luk, and B. Duan, "Multiobjective optimal antenna synthesis for microwave wireless power transmission," *IEEE Transactions on Antennas and Propagation*, Vol. 67, No. 4, 2739–2744, 2019.
13. Brown, W. C. and E. E. Eves, "Beamed microwave power transmission and its application to space," *IEEE Transactions on Microwave Theory & Techniques*, Vol. 40, No. 6, 1239–1250, 1992.
14. Zhang, S., L. W. Song, B. Y. Duan, et al., "Aperture amplitude field integrated design of receiving and transmitting antenna for microwave power transmission," *IEEE Antennas and Wireless Propagation Letters*, Vol. 19, No. 7, 1216–1220, 2020.
15. Song, C. M., S. Trinh-Van, S. H. Yi, et al., "Analysis of received power in RF wireless power transfer system with array antennas," *IEEE Access*, Vol. 9, 76315–76324, 2021.
16. Li, J. and Y. Tan, "A novel receiving antenna array layout method for microwave power transmission," *Progress In Electromagnetics Research M*, Vol. 108, 187–200, 2022.
17. Li, X., B. Duan, J. Zhou, et al., "Planar array synthesis for optimal microwave power transmission with multiple constraints," *IEEE Antennas and Wireless Propagation Letters*, Vol. 16, 70–73, 2017.
18. Wan, S. and K. Huang, "Methods for improving the transmission-conversion efficiency from transmitting antenna to rectenna array in microwave power transmission," *IEEE Antennas and Wireless Propagation Letters*, Vol. 17, No. 4, 538–542, 2018.
19. Xiong, Z., Z. Xu, S. Chen, et al., "Subarray partition in array antenna based on the algorithm X," *IEEE Antennas and Wireless Propagation Letters*, Vol. 12, No. 12, 906–909, 2013.
20. Zheng, Z., Y. Yan, L. Zhang, et al., "Research on genetic algorithm of antenna arrays beam shaping with side lobe suppression," *Journal of Electronics and Information Technology*, Vol. 39, No. 3, 690–696, 2017.
21. Banerjee, C. and R. Sawal, "PSO with dynamic acceleration coefficient based on mutiple constraint satisfaction: Implementing fuzzy inference system," *2014 International Conference on Advances in Electronics Computers and Communications*, 1–5, 2014.
22. Kojima, S., N. Shinohara, and T. Mitani, "Synthesis loss in receiving array antennas and transmission efficiency in the Fresnel region," *Wireless Power Transfer*, Vol. 4, No. 2, 120–131, 2017.
23. Rocca, P., G. Oliveri, and A. Massa, "Innovative array designs for wireless power transmission," *International Microwave Workshop Series on Innovative Wireless Power Transmission: Technologies, Systems, and Applications*, 279–282, 2011.
24. Miao, A., X. Shi, J. Zhang, et al., "A modified particle swarm optimizer with dynamical inertia weight," *Fuzzy Information and Engineering Volume 2. Advances in Intelligent and Soft Computing*, Vol. 62, 767–776, 2009.
25. Guo, Q., C. Chen, and Y. Jiang, "An effective approach for the synthesis of uniform amplitude concentric ring arrays," *IEEE Antennas Wireless Propag. Lett.*, Vol. 16, 2558–2561, 2017.

26. Zhou, H. W., X. X. Yang, and S. Rahim, "Synthesis of the sparse uniform-amplitude concentric ring transmitting array for optimal microwave power transmission," *International Journal of Antennas & Propagation*, Article ID 8075318, 8 pages, 2018.
27. Oliveri, G., L. Poli, and A. Massa, "Maximum efficiency beam synthesis of radiating planar arrays for wireless power transmission," *IEEE Transactions on Antennas and Propagation*, Vol. 61, No. 5, 2490–2499, 2013.